# Low silica activity for hydrogen generation during serpentinization: an example of natural serpentinites in the Mineoka ophiolite complex, central Japan

Ikuo Katayama*, Iori Kurosaki[1], and Ken-ichi Hirauchi

*Department of Earth and Planetary Systems Science, Hiroshima University, Higashi-Hiroshima 739-8526, Japan*

*Corresponding author:

Tel: +81-824-24-7468, Fax: +81-824-24-0735,

E-mail: katayama@hiroshima-u.ac.jp

[1]Now at Graduate School of Social and Cultural Studies, Kyushu University, Fukuoka 812-8581, Japan

**Abstract**

The textural evolution in the serpentnite of the Mineoka ophiolite complex has been investigated to constrain the natural environment for hydrogen production in the serpentinite-hosted hydrothermal vent systems. Textural relations of the serpentinites from the Mineoka ophiolite indicate at least two stages in the process of serpentinization, with the replacement of olivine by a mesh texture of serpentine and brucite, followed by the development of magnetite-bearing or -free serpentine veins. The generation of hydrogen during serpentinization, which accompanies the formation of magnetite, involves a silica-depletion reaction, as evidenced by the low abundance of serpentine in the magnetite-bearing veins and the absence of magnetite in pseudomorphs of orthopyroxene. Direct evidence for the production of hydrogen and strongly reducing conditions is provided by $CH_4$ and $H_2$-bearing inclusions in relic olivine crystals; the production of methane and hydrogen may have provided a suitable environment for microbial activity in hydrothermal vent systems along the seafloor. Our results indicate that low silica activity plays a key role in the generation of hydrogen during serpentinization, and that low silica activity environments are possible in olivine-rich rocks such as dunite, or during local disequilibrium in other silica-poor rocks in the mantle lithosphere.

*Keywords: serpentinite, magnetite, hydrogen, silica activity, hydrothermal vent system, microbial community*

## 1. Introduction

Microbial communities are known to exist in the vicinity of the seafloor where they take part in various chemical reactions (e.g., Corliss et al., 1979; Spiess et al., 1980; Baross and Hoffman, 1985; Takai, 2004). Remarkable submarine ecosystems have been reported in the serpentinite-hosted hydrothermal fields where hydrogen is a key product for the microbial activity (e.g., Kelley et al., 2001, 2005; Holm and Charlou, 2001; Nakamura et al., 2009). Serpentinites are formed by reaction between hydrothermal fluids and mantle rocks, and hydrogen and methane are released in the extremely reducing conditions. It is now generally thought that hydrothermal vents associated with serpentinized rocks played a key role in the genesis of life in the early oceans (e.g., Sleep et al., 2004; Martin et al., 2008), sparking renewed interest in water-rock interactions in the vicinity of the seafloor. It is important, therefore, to study the process of serpentinization, which is currently not well constrained in natural rock samples.

Under strongly reducing conditions, the formation of magnetite always generates hydrogen during serpentinization, following reactions such as:

$$3Fe_2SiO_4 + 2H_2O = 2Fe_3O_4 + 3SiO_2 + 2H_2 \quad (1)$$

olivine + water = magnetite + silica + hydrogen.

Based on mineralogical and textural observations, a two stage model for serpentinization has been proposed, involving the early formation of brucite and serpentine followed by magnetite formation (e.g., Toft et al., 1990; Oufi et al., 2002;

59 Bach et al., 2006; Beard et al., 2009). The first reaction is:

60

61 $2(Mg, Fe)_2SiO_4 + 3H_2O = (Mg, Fe)_3Si_2O_5(OH)_4 + (Mg, Fe)(OH)_2$ (2)

62 olivine + water = serpentine + brucite.

63

64 The products of this reaction often form a mesh texture after olivine.

65 For the second stage of the process of serpentinization, a number of reactions have
66 been suggested, depending on the degree of silica activity. For example, Bach et al.
67 (2006) proposed that the formation of magnetite, during the breakdown of ferroan
68 brucite, is facilitated by relatively high silica activity, as follow:

69

70 $9Fe(OH)_2 + 4SiO_2 = 2Fe_3Si_2O_5(OH)_4 + Fe_3O_4 + 4H_2O + H_2$ (3)

71 brucite + silica = serpentine + magnetite + water + hydrogen.

72

73 In contrast, Frost and Beard (2007) reported that the second stage of serpentinization
74 reflects the inherent instability of ferroan serpentine during low silica activity, with the
75 breakdown of the ferrous component to form magnetite, as follows:

76

77 $Fe_3Si_2O_5(OH)_4 = Fe_3O_4 + 2SiO_2 + H_2O + H_2$ (4)

78 serpentine = magnetite + silica + water + hydrogen.

79

80 Thus, the conditions for magnetite formation during serpentinization remain unclear,

81 even though the process plays a key role in microbial activity in the extremely reducing
82 conditions of the seafloor.
83 In this study, we described the mineralogical evolution of serpentinized peridotites
84 from the Mineoka ophiolite complex, central Japan, discuss the processes of hydrogen
85 generation during serpentinization, and comment on the environments which hosted
86 microbial activity in these extreme conditions on Earth.
87
88 **2. Sample description and petrography**
89 Serpentinites were collected from the Mineoka belt, central Japan. This belt is
90 recognized as an accreted ophiolite fragment with a mid-oceanic ridge affinity (e.g.,
91 Ogawa and Taniguchi, 1988; Sato et al., 1999). Peridotites in the Mineoka belt are
92 mostly serpentinized as a result of extensive hydrothermal activity, and they are
93 generally massive except near basaltic blocks. These ultramafic rocks contain relict
94 minerals, including olivine ($Fo_{90-93}$), orthopyroxene ($En_{89-91}$), and Cr-rich spinel.
95 Chemical compositions, and the lack of cumulate textures, suggest that the rocks
96 originated as a residue from partial melting (Sato and Ogawa, 2000).
97 The massive serpentinites are characterized by mesh textures, which are
98 pseudomorph after olivine. Orthopyroxene pseudomorphs made of bastite are also
99 locally observed. Serpentine minerals in these pseudomorphs are lizardite and/or
100 chrysotile, as identified by laser Raman spectroscopy and TEM observations (Hirauchi
101 et al., 2010). The occurrence of low-temperature serpentines is a common feature of
102 serpentinized peridotites on the seafloor (e.g., Wicks and Whitaker, 1977). Most

serpentinites contain magnetite as either stringers or patches in late-stage veins that crosscut the mesh texture after olivine, but these veins do not directly contact with relict olivine crystals (Fig. 1A, B). Orthopyroxene is commonly replaced by serpentine (bastite), but magnetite is never observed in the serpentine-filled veins within orthopyroxene pseudomorphs (Fig. 1C, D). Chemical mapping shows the existence of several domains within the serpentine-filled veins that cut the replaced olivine. The domains are disposed as bands symmetrically about the center of the vein (Fig. 2). Most magnetite occurs in the Fe-rich central domains, surrounded by relatively Si-rich and Fe-poor domains.

The veins are composed of multiple phases on the submicron scale, and electron microprobe analysis (with a focused 3 $\mu$m beam) was used to identify the chemical compositions of each domain. The compositions of the serpentine-filled veins cutting olivine and orthopyroxene are shown in Figure 3 and Table 1. Microprobe analyses indicate that the veins in olivine are mixtures of serpentine and brucite; the compositions fall on a straight line that connects stoichiometric serpentine and brucite (Fig. 3A). Similar mixtures of brucite and serpentine have been documented from the IODP drilled troctolites (Beard et al., 2009) and the Oman ophiolite complex (Baronnet and Boudier, 2001). The domains outside the veins (domain 1) exhibits the typical mesh texture of replaced olivine, and it has a composition relatively rich in Fe and poor in Si, reflecting the high concentration of brucite near the olivine-mesh contact. The olivine pseudomorphs are cut by later stage veins (Fig. 1), which are also mixtures of brucite and serpentine with distinct ratios of these minerals (Table 1). The veins are composed

of relatively Si-rich bands with high abundance of serpentine (domain 2), and magnetite-bearing Si-poor domains in center portion (domain 3). Based on simple two end-member calculations, serpentine abundance is 97-99% in the Si-rich domains and 84-90% in the Si-poor domains, respectively.

Laser Raman analysis reveals that serpentines in domain 1 and 3 are lizardite characterized by double bands at 3685 and 3705 $cm^{-1}$, whereas those in domain 2 are mainly composed of chrysotile at 3701 $cm^{-1}$ with additional bands of brucite (Fig. 4). Chrysotile is known to appear at isotropic stress environments of fluid-filled voids and pores, although it is highly unstable under stress associated with expansion, flattening and shear (Evans, 2004). Fe-Ni alloys, including awaruite ($FeNi_3$), are also identified in association with magnetite in the central domains (domain 3).

Serpentine-filled veins cutting orthopyroxene have a distinctive chemical composition, and in contrast to those cutting olivine, they do not contain different chemical domains. They have a substantially higher $Al_2O_3$ content (up to 2.9 wt%) than those cutting olivine, and the sum of tetrahedral cations, silicon and aluminum, is significantly higher than in the serpentine end-member, indicating the presence of talc (Fig. 3B).

The Fe contents of these serpentine-filled veins are little scattered; $X_{Fe}$ is ranging 0.04-0.12 after olivine, and $X_{Fe}$ is 0.06-0.15 after orthopyroxene (Fig. 5). In the veins of olivine pseudomorph, the magnetite-free domain (domain 2) tends to show lower Fe contents compared to the other domains. Such variation may reflect the dominant serpentine phase, since the domain 2 is mainly composed of chrysotile whereas lizardite

147 is a stable serpentine form in the domain 1 and 3 as identified by the Raman spectra.
148 Similar trend of lower $X_{Fe}$ in chrysotile has been also reported in the serpentinized
149 olivine websterite from the Canyon Mountain complex (Evans et al., 2009).
150
151 **3. Magnetite-forming reactions**
152 Textural relationships clearly indicate at least two stages in the process of
153 serpentinization in the Mineoka ophiolite complex, involving first the formation of a
154 serpentine mesh texture after olivine, then magnetite-bearing serpentine-filled veins.
155 The absence of magnetite in the mesh texture suggests reaction (2) as the first-stage
156 process in the process of serpentinization of the Mineoka peridotites. The mesh texture
157 is crosscut by magnetite-bearing veins, which are composed of two chemically distinct
158 layers (Fig. 3A). Although two principle reactions of (3) and (4) are possible, it is likely
159 that reaction (4) was responsible for the formation of the magnetite, with magnetite in
160 the Si-poor domains, representing the serpentine-out reaction. This reaction is also
161 consistent with the low silica activity imposed by the brucite-serpentine assemblage
162 (Fig. 6). Although the Fe-Mg exchange potential has been recently suggested to control
163 the formation of magnetite during serpentinization (Evans, 2008), this mechanism is
164 unlikely in our natural systems. Because the chemical potential of iron is similar
165 between the magnetite-bearing and -free serpentine-filled veins, and the variations of Fe
166 value are probably results of the stable serpentine phase in the Mineoka serpentinites.
167 These lines of evidences suggest that low silica activity is likely to facilitate the reaction
168 of ferroan serpentine to form magnetite. One consequence of magnetite formation is the

169 imposition of extremely reducing conditions on the system, and in turn, this resulted in
170 the formation of iron alloys in the magnetite-bearing domains. Assemblages of sulfide
171 and native-metal minerals in the Mineoka serpentinites also indicate low $f_{O2}$ and $f_{S2}$
172 during serpentinization (Sato and Ogawa, 2000).

173 The other key point is the absence of magnetite in the bastites (orthopyroxene
174 pseudomorphs). The serpentine veins cutting the orthopyroxene have higher tetrahedral
175 cations than those cutting serpentinized olivine, and they contain a mixture of serpentine
176 and talc (Fig. 3B), which contrasts with the brucite-serpentine mixture in veins cutting
177 olivine. The hydration of orthopyroxene is probably represented by the reaction:

178

179 $6(Mg, Fe)SiO_3 + 3H_2O = (Mg, Fe)_3Si_2O_5(OH)_4 + (Mg, Fe)_3Si_4O_{10}(OH)_2$ (5)
180 orthopyroxene + water = serpentine + talc.

181

182 The talc then releases silica into the hydrothermal fluid by the following reaction:

183

184 $(Mg, Fe)_3Si_4O_{10}(OH)_2 + H_2O = (Mg, Fe)_3Si_2O_5(OH)_4 + SiO_2$ (6)
185 talc + water = serpentine + silica.

186

187 The production of serpentine and talc is a result of an approximately two orders of
188 magnitude higher silica activity than that needed for the production of the assemblages
189 serpentine and brucite after olivine (Fig. 6). Magnetite is absent from the serpentine and
190 talc assemblages replacing orthopyroxene, whereas the Fe values are similar for
191 pseudomorphs after both olivine and orthopyroxene (Fig. 5), indicating that a low silica

192 activity is crucial for the formation of magnetite during serpentinization. During the
193 hydration of harzburgite, where orthopyroxene and olivine coexist, silica tends to move
194 from talc-bearing portions to brucite-bearing portions. Variations in silica activity
195 during serpentinization of peridotite depend on the relative rates of the hydration of
196 olivine and orthopyroxene, and on fluid flow in the rocks. The occurrence of talc after
197 orthopyroxene in the Mineoka serpentinites provides evidence for preservation of a
198 large gradient in silica activity as the result of limited fluid pathways in the rocks. In the
199 case of external supply of silica, such a model implies that olivine may hydrate without
200 forming magnetite.
201
202 **4. $H_2$- and $CH_4$-bearing fluid inclusions**
203 Fluid-like inclusions are found in the relict olivine crystals. The inclusions are
204 randomly distributed, but do not occur in secondary microfractures. The inclusions are
205 generally less than 20 $\mu$m in size, and mostly contain two-phase inclusions (Fig. 7). We
206 prepared doubly polished sections for laser Raman analysis to avoid contamination
207 from adhesive agents. Raman spectra of the inclusions were obtained using the 514.5
208 nm line of an Ar laser (RENISHAW inVia Reflex). The laser beam was focused to a
209 spot size of approximately 1 $\mu$m, and the spectra were scanned from 200 to 4400 $cm^{-1}$.
210 The micro-inclusions were characterized by a strong band at 3698 $cm^{-1}$, in addition to
211 the host olivine bands at 822 and 854 $cm^{-1}$ (Fig. 8A). The 3698 $cm^{-1}$ band is typical of
212 chrysotile (Rinaudo et al., 2003), which indicates the inclusions are composed mainly of
213 serpentine precipitated at low temperatures. These inclusions contain weak but

detectable bands of $CH_4$ at 2916 $cm^{-1}$ and $H_2$ at 4156 $cm^{-1}$ (Fig. 8B, D). Although these vapor phases have been mostly removed from the matrix assemblages, the inclusions provide direct evidence of methane and hydrogen in the fluids during serpentinization. Phase equilibria indicates that the $CH_4$-$H_2$ bearing fluids were trapped under equilibrium conditions at temperatures below 300°C, where lizardite and chrysotile are stable (Evans, 2004), and under markedly reducing conditions. The absence of $CO_2$ as a fluid component suggests an extensive reduction of $CO_2$ to $CH_4$ in the $H_2$-rich hydrothermal vent systems. This is consistent with typical serpentine-hosted hydrothermal systems that exhibit high $CH_4$ concentrations along with an enrichment in $H_2$ (Donval et al., 1997; Charlou et al., 2002).

## 5. Implications and conclusions

The textural evolution of the Mineoka serpentinites shows that magnetite does not form directly from olivine. The magnetite-forming reaction involves a silica-out reaction, as witnessed by the lower abundance of serpentine in the magnetite-bearing veins, and the absence of magnetite in pseudomorphs after orthopyroxene. This suggests that the occurrence of magnetite is possible when there is a significant low silica activity in the fluids, implying that the system had locally evolved to lower silica activity during serpentinization. The magnetite formation results in the production of hydrogen and strongly reducing conditions, which may potentially support microbial activity in the vicinity of the seafloor (e.g., Kelley et al., 2001; Takai et al., 2004; McCollom, 2007). The $CH_4$ and $H_2$-bearing inclusions in relics of olivine provide direct

236 evidence for the presence of $CH_4$ and $H_2$-rich hydrothermal vents during
237 serpentinization, although those vapor phases have been almost entirely obliterated from
238 the matrix assemblages. Our results indicate that, in addition to low oxygen fugacity,
239 low silica activity is a key to generate hydrogen during serpentinization, and this is
240 possible in rocks dominated by olivine, such as dunite, or locally, as a result of
241 disequilibrium, in other silica-poor mantle rocks.
242
243 **Acknowledgements**
244 We thank Y. Takahashi, T. Naganuma and K. Michibayashi for comments and
245 discussions. We also thank K. Okuzawa for help in the sample collection, Y. Shibata for
246 microprobe analysis, and H. Hidaka and T. Hirotaka for laser Raman analysis.
247 Constructive review by B. R. Frost and an anonymous reviewer are appreciated for
248 improving the manuscript. This research was supported by the Japan Society for the
249 Promotion of Science (JSPS).
250
251 **References**
252 Bach, W., Paulick, H., Garrido, C.J., Ildefonse, B., Meurer, W.P., Humphris, S.E., 2006.
253 Unraveling the sequence of serpentinization reactions: petrography, mineral
254 chemistry, and petrophysics of serpentinites from MAR 15°N (ODP Leg 209,
255 Site1274). Geophys. Res. Lett. 33, L13306. doi:10.1029/2006GL025681.
256 Baronnet, A., Boudier, F., 2001. Microstructural and microchemical aspects of
257 serpentinization, Lunar Planet. Sci. XI, Abst. 3382.

258 Baross J.A, Hoffman S.E., 1985. Submarine hydrothermal vents and associated gradient
259 environments as sites for the origin and evolution of life. Orig. Life Evol. Biosph.
260 15, 327–345.
261 Beard, J., Frost, B.R., Fryer, P., McCaig, A., Searle, R., Ildefonse, B., Zinin, P., Sharma,
262 S.K., 2009. Onset and Progression of Serpentinization and Magnetite Formation in
263 Olivine-richTroctolite from IODP Hole U1309D. J. Petrol. 50, 387-403.
264 Charlou, J.L., Donval, J.P., Fouquet, Y., Jean-Baptiste, P., Holm, N., 2002.
265 Geochemistry of high H2 and CH4 vent fluids issuing from ultramafic rocks at the
266 Rainbow hydrothermal field (36°14′ N, MAR). Chem. Geol. 191, 345–359.
267 Corliss, J.B., Dymond, J., Gordon, L.I., Edmond, J.M., von Harzen, R.P., Ballard, R.D.,
268 Green, K., Williams, D., Bainbridge, A., Crane, K. van Andel, T.H., 1979.
269 Submarine thermal springs on the Galapagos Rift. Science 203, 1073–1083.
270 Donval, J.P., Charlou, J.L., Donville, E., Radford-Knoery, J., Fouquet, Y., Panzevera,
271 E., Jean-Baptiste, P., Stievenard, M., German, C., FLORES Cruise Scientific Party,
272 1997. High H2 and CH4 content in hydrothermal fluids from Rainbowsite newly
273 sampled at 36°14′ Non the AMAR segment Mid-Atlantic Ridge (diving FLORES
274 cruise, July 1997): Comparison with other MAR sites. EOS Trans. AGU 78,
275 FallMeet. Suppl., Abstract V51E-06.
276 Evans, B.W., 2004. The serpentinite multi-system revisited; chrysotile is metastable. Int.
277 Geol. Rev. 46, 479-506.
278 Evans, B.W., 2008. Control of the products of serpentinization by the $Fe^{2+}Mg_{-1}$
279 exchange potential of olivine and orthopyroxene. J. Petrol. 49, 1873-7887..

280 Evans, B.W., Kuehner, S.M., Chopelas, A., 2009. Magnetite-free, yellow lizardite
281 serpentinization of olivine websterite, Canyon Mountain complex, NE. Oregon. Am.
282 Mineral. 94, 1731-1734.
283 Frost, B.R., Beard, J.S., 2007. On silica activity and serpentinization. J. Petrol. 48,
284 1351–1368.
285 Frost, B.R., Beard, J.S., 2008. On silica activity and serpentinization: Errata. J. Petrol.
286 49, 1253.
287 Hirauchi, K., Katayama, I., Uehara, S., Miyahara, M., Takai, Y., 2010. Inhabitation of
288 subduction thrust earthquakes by low-temperature plastic flow in serpentine. Earth
289 Planet. Sci. Lett. 295, 349-357.
290 Holm, N.G., Charlou, J.L., 2001. Initial indications of abiotic formation of
291 hydrocarbons in the Rainbow ultramafic hydrothermal system, Mid-Atlantic Ridge,
292 Earth Planet. Sci. Lett. 191, 1–8.
293 Kelley, D.S., Karson, J.A., Blackman, D.K., Fru¨h-Green, G.L., Butterfield, D.A.,
294 Lilley, M.D., Olson, E.J., Schrenk, M.O., Roe, K.K., Lebon, G.T., Rivizzigno, P.,
295 the AT3-60 Shipboard Party, 2001. An off-axis hydrothermal vent field near the
296 Mid-Atlantic Ridge at 30°N. Nature 412, 145–149.
297 Kelley, D.S., Karson, J.A., Fru¨h-Green, G.L., Yoerger, D.R., Shank, T.M., Butterfield,
298 D.A., Hayes, J.M., Schrenk, M.O., Olson, E.J., Proskurowski, G., Jakuba, M.,
299 Bradley, A., Larson, B., Ludwig, K., Glickson, D., Buckman, K., Bradley, A.S.,
300 Brazelton, W.J., Roe, K., Elend, M.J., Delacour, A., Bernasconi, S.M., Lilley, M.D.,

301 Baross, J.A., Summons, R.E., Sylva, S.P., 2005. A serpentinite-hosted ecosystem:
302 the Lost City hydrothermal field. Science 307, 1428–1434.
303 Martin, W., Baross, J., Kelley, D.S., Russell, M.J., 2008. Hydrothermal vents and the
304 origin of life: Nature Rev. Microbio. 6, 805-814.
305 McCollom, T.M., 2007. Geochemical constraints on sources of metabolic energy for
306 chemolithoautotrophy in ultramafic-hosted deep-sea hydrothermal systems,
307 Astrobiology 7, 933–950.
308 Nakamura, K., Morishita, T., Bach, W., Klein, F., Hara, K., Okino, K., Takai, K.,
309 Kumagai, H., 2009. Serpentinized troctolites exposed near the Kairei Hydrothermal
310 Field, Central Indian Ridge: Insights into the origin of the Kairei hydrothermal fluid
311 supporting a unique microbial ecosystem. Earth Planet. Sci. Lett. 208, 128-136.
312 Ogawa, Y., Taniguchi, H., 1988. Geology and tectonics of the Miura-Boso Peninsulas
313 and adjacent area. Modern Geology 12, 147-168.
314 Oufi, O., Cannat, M., Horen, H., 2002. Magnetic properties of variably serpentinized
315 abyssal peridotite. J. Geophys. Res. 107, 10.1029/2001JB000549.
316 Rinaudo, C., Gastaldi, D., Belluso, E., 2003. Characterization of chrysotile, antigorite
317 and lizardite by FT-Raman spectroscopy. Can. Mineral. 41, 883-890.
318 Sato, H., Taniguchi, H., Takahashi, N., Mohiuddin, M.M., Hirano, N., Ogawa, Y., 1999.
319 The origin of the Mineoka ophiolite. J. Grograph., Tokyo Geograph. 108, 177-189
320 (Japanese with English abstract).
321 Sato, H., Ogawa, Y., 2000. Sulfide minerals as an indicator for petrogenesis and
322 serpentinization of peridotites: An example from Hayama-Mineoka belt, central

323 Japan. In: Dilek, Y., Moores, E., Elton, D., Nicolas, A. (Eds.), Ophiolites and
324 oceanic crust: New insights from field studies and ocean drilling program,
325 Geological Society of America, 349, 427-437.
326 Sleep, N.H., Meibom, A., Fridriksson, T., Coleman, R.G., Bird, D.K., 2004. $H_2$-rich
327 fluids from serpentinization: geochemical and biotic implications. Proc. Natl. Acad.
328 Sci. USA 101, 12818–12823.
329 Spiess, F.N., Macdonald, K.C., Atwater, T., Ballard, R., Carranza, A., Cordoba, D., Cox,
330 C., Daiz Garcia, V.M., Francheteau, J., Guerrero, J., Hawkins, J., Haymon, R.,
331 Hessler, R., Juteau, T., Kastner, M., Larson, R., Luyendyk, B., Macdougall, J.D.,
332 Miller, S., Normark, W., Orcutt, J., Rangin, C., 1980. East Pacific Rise: hot springs
333 and geophysical experiments. Science 207, 1421–1433.
334 Takai, K., Gamo, T., Tsunogai, U., Nakayama, N., Hirayama, H., Nealson, K.H.,
335 Horikoshi, K., 2004. Geochemical and microbiological evidence for a
336 hydrogen-based, hyperthermophilic subsurface lithoautotrophic microbial
337 ecosystem (HyperSLiME) beneath an active deep-sea hydrothermal field.
338 Extremophiles 8, 269–282.
339 Toft, P.B., Arkani-Hamed, J., Haggerty, S.E., 1990. The effects of serpentinization on
340 density and magnetic susceptibility: a petrophysical model. Phys. Earth Planet. Int.
341 65, 137–157.
342 Wicks, F.J., Whittaker, E.J.W., 1977. Serpentine texture and serpentinization. Can.
343 Mineral. 13, 227–243.
344

345 **Figure captions**

346 **Figure 1.** Photomicrographs of serpentinized peridotites from the Mineoka ophiolite
347 complex, showing serpentine after olivine (A: cross-polarized light, B: plane-polarized
348 light) and after orthopyroxene (C: cross-polarized light, D: plane-polarized light).
349 Magnetite occurs in the serpentine-filled veins that crosscut the mesh texture replacing
350 olivine (A, B), whereas magnetite is absent in the serpentine-filled veins that crosscut
351 orthopyroxene. Mineral abbreviations are, Ol: olivine, Mgt: magnetite, Serp: serpentine,
352 Brc: brucite, Opx: orthopyroxene, and Tlc: talc.

353

354 **Figure 2.** Elemental mapping for Mg, Si, and Fe in serpentinized area near olivine.
355 Colors correspond to the X-ray intensity, where bluish and reddish colors represent low
356 and high intensities, respectively. The serpentinized areas are divided into three
357 domains; the first is the mesh texture that replaces olivine (domain 1), the second is the
358 magnetite-free material on either side of the central magnetite-bearing zone of
359 serpentine veins (domain 2), and the third is the magnetite-bearing center of the
360 serpentine veins (domain 3).

361

362 **Figure 3.** Chemical composition of serpentine filled veins after olivine (A) and
363 orthopyroxene (B), as a function of Si + Al and Mg + Fe cations per 7 oxygens. The
364 variations in chemical composition in domains of olivine replacement suggest mixtures
365 of brucite and serpentine, whereas the composition where orthopyroxene has been
366 replaced indicates a mixture of serpentine and talc. In serpentine-filled veins cutting

olivine (A), the magnetite-bearing domains tend to have a higher brucite content than the magnetite-free domains.

**Figure 4.** Raman spectra of the serpentine-filled veins. (A) Mesh texture after olivine is represented by lizardite at double bands of 3685 and 3705 $cm^{-1}$, (B) magnetite-free veins after olivine are characterized by chrysotile at 3701$cm^{-1}$ as well as smaller bands of brucite at 3643 $cm^{-1}$.

**Figure 5.** Chemical composition of serpentine filled veins after olivine and orthopyroxene, as a function of Fe value and Si + Al cations per 7 oxygens. The variation may reflect the stable serpentine phase (lizardite or chrysotile) in addition to the brucite abundance in the veins.

**Figure 6.** (A) A phase composition in the $MgO$-$SiO_2$-$H_2O$ system and (B) silica activity in serpentinized areas calculated for a pressure of 1 kbar (Frost and Beard, 2008). The serpentine-talc assemblage after orthopyroxene indicates approximately two orders of magnitude higher silica activity than the serpentine-brucite assemblage after olivine. Quartz (Qtz), talc (Tlc), enstatite (En), forsterite (Fo), serpentine (Serp), brucite (Brc), olivine (Ol), orthopyroxene (Opx).

**Figure 7.** Photomicrographs of fluid inclusions in olivine crystals (plane-polarized light), which are mostly filled with serpentine.

389

390 **Figure 8.** Raman spectra of fluid inclusions in olivine. The spectrum as a whole (A)
391 shows a band characterized by chrysotile at 3698 $cm^{-1}$, in addition to the host olivine
392 bands at 822 and 854 $cm^{-1}$, suggesting that inclusions are mainly composed of
393 low-temperature serpentine. Enlarged Raman spectra (B, D) show weak but detectable
394 evidence for the vapor phases $CH_4$ (2916 $cm^{-1}$) and $H_2$ (4516 $cm^{-1}$) in the inclusions.

395

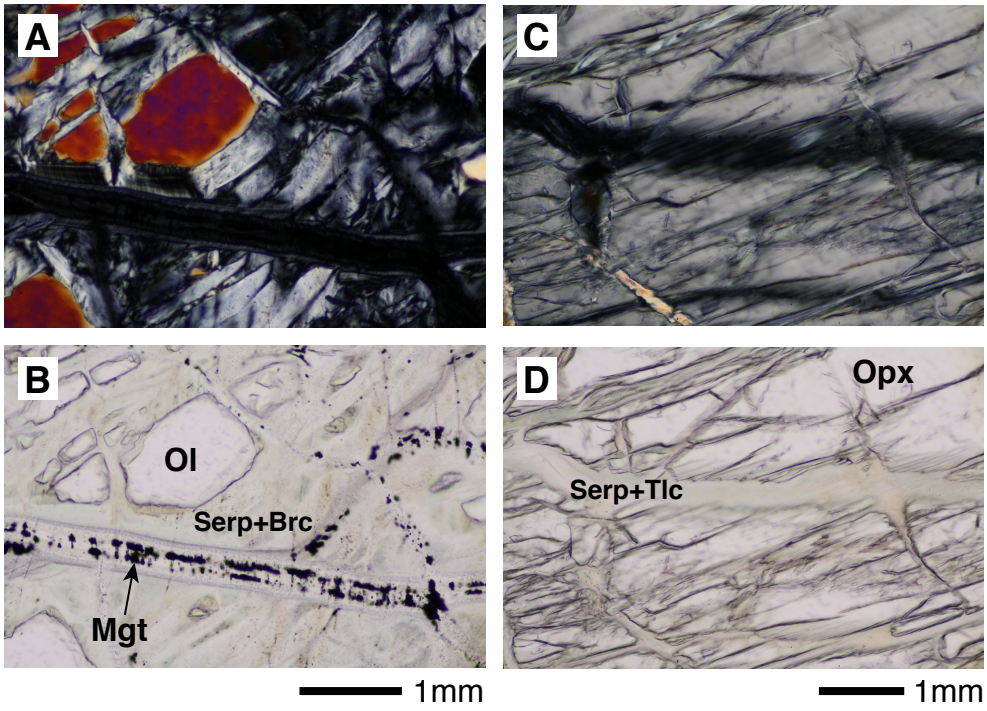


Figure 1. Katayama et al.

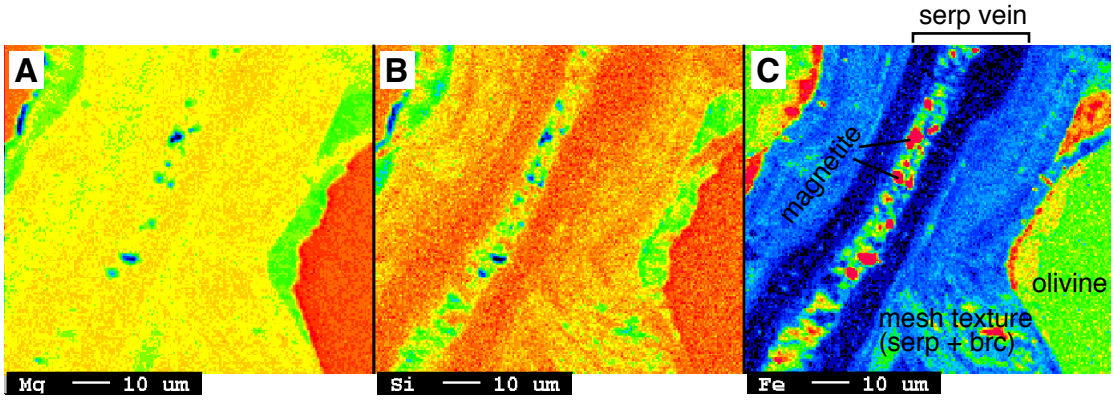


Figure 2. Katayama et al.

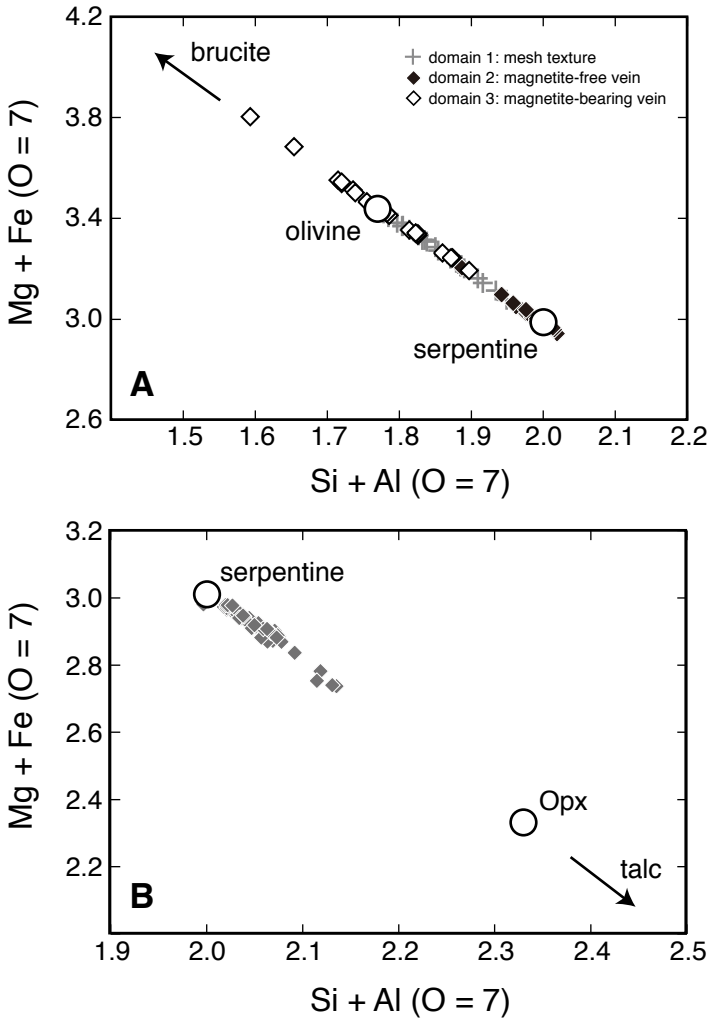


Figure 3. Katayama et al.

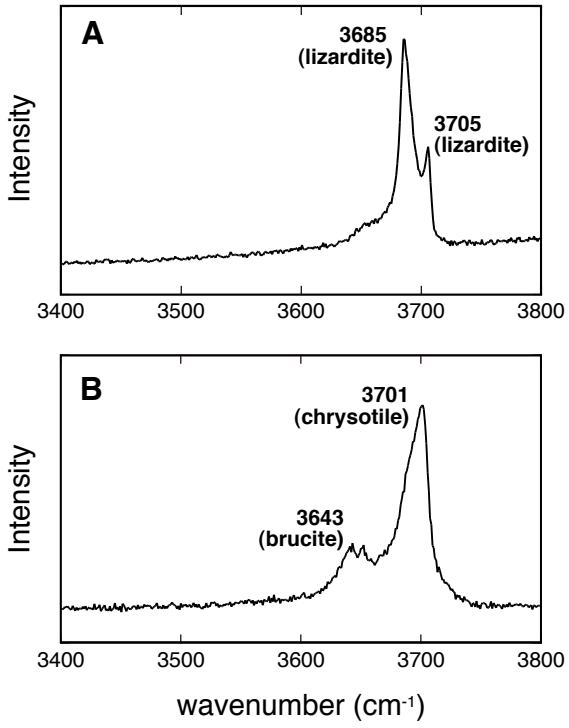


Figure 4. Katayama et al.

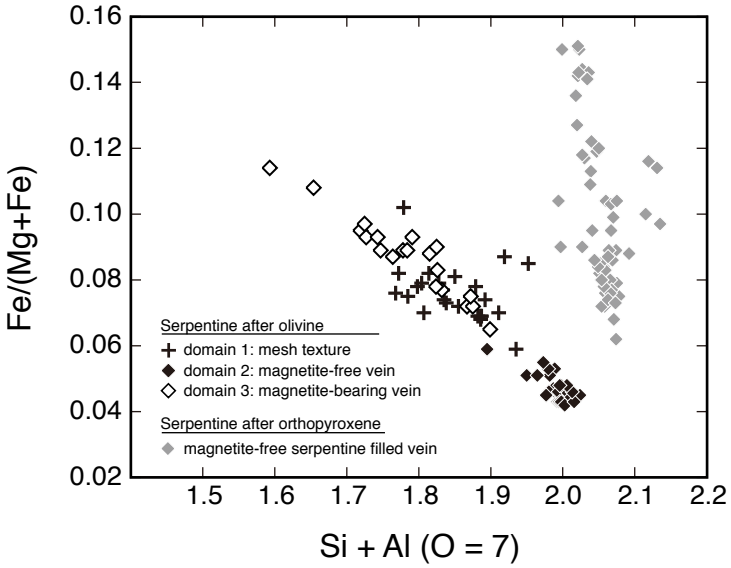


Figure 5. Katayama et al.

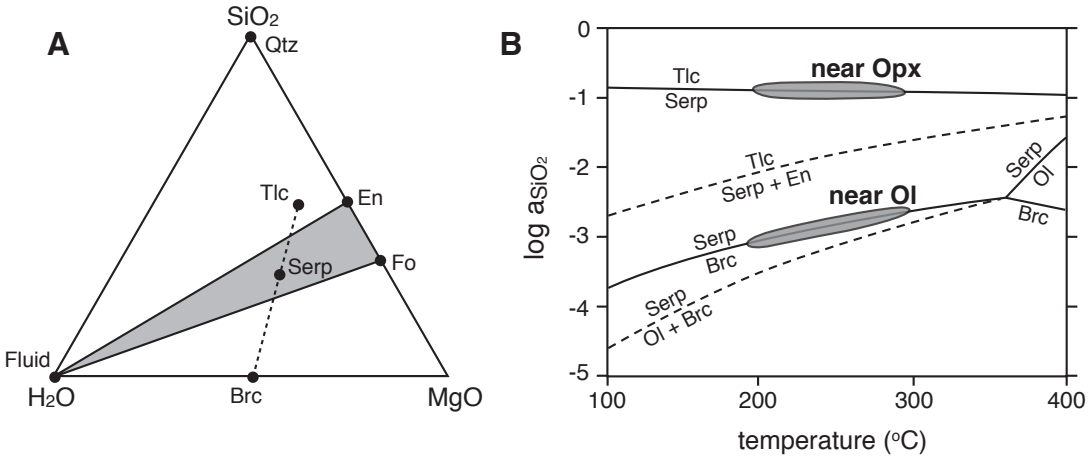


Figure 6. Katayama et al.

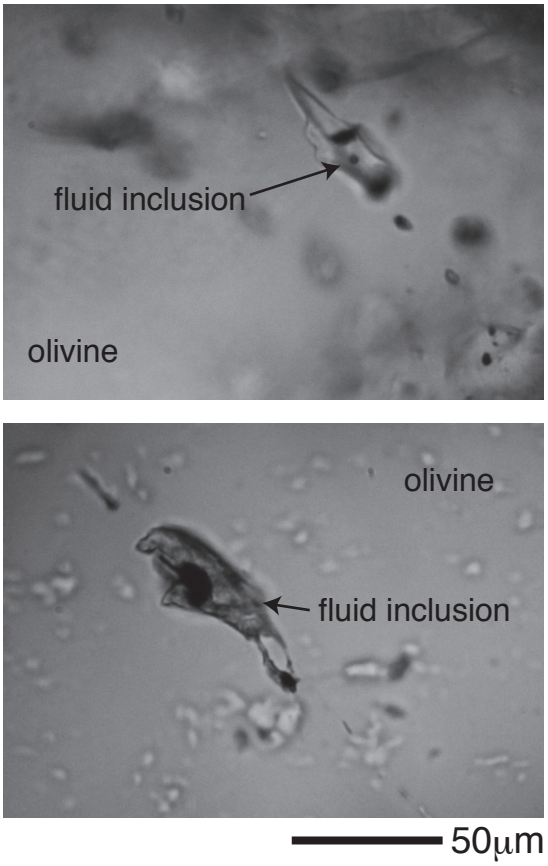


Figure 7. Katayama et al.

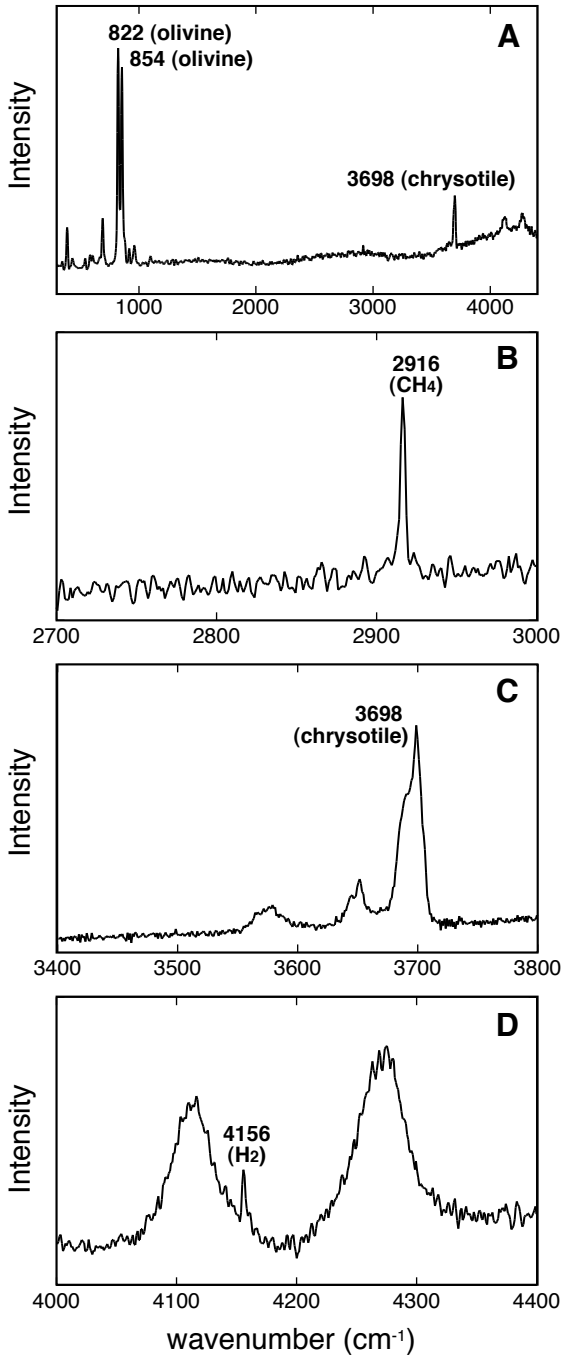


Figure 8. Katayama et al.

Table 1. Chemical compositions of serpentines after olivine and orthopyroxene

| | | serpentines after olivine | | | | | |
|---|---|---|---|---|---|---|---|
| | olivine | domain 1 | domain 2 | domain 3 | Opx | serpentines after Opx | serpentines after Opx |
| $SiO_2$ | 40.64 | 38.84 | 41.16 | 34.64 | 55.65 | 38.18 | 39.89 |
| $TiO_2$ | 0.04 | 0.00 | 0.03 | 0.04 | 0.10 | 0.07 | 0.02 |
| $Al_2O_3$ | 0.02 | 0.02 | 0.12 | 0.16 | 3.07 | 2.97 | 2.30 |
| FeO* | 8.50 | 5.35 | 3.20 | 7.15 | 5.54 | 6.01 | 6.28 |
| MnO | 0.16 | 0.07 | 0.03 | 0.08 | 0.17 | 0.23 | 0.18 |
| $Cr_2O_3$ | 0.06 | 0.01 | 0.03 | 0.01 | 0.69 | 0.85 | 0.27 |
| MgO | 50.09 | 40.16 | 39.79 | 41.89 | 33.87 | 36.32 | 36.28 |
| CaO | 0.05 | 0.06 | 0.03 | 0.02 | 1.13 | 0.05 | 0.07 |
| $Na_2O$ | 0.01 | 0.03 | 0.01 | 0.01 | 0.02 | 0.00 | 0.00 |
| $K_2O$ | 0.00 | 0.00 | 0.03 | 0.01 | 0.00 | 0.00 | 0.00 |
| NiO | 0.41 | 0.30 | 0.07 | 0.00 | 0.14 | 0.11 | 0.04 |
| Total | 99.98 | 84.83 | 84.50 | 84.01 | 100.37 | 84.79 | 85.33 |
| | | | | | | | |
| Cation per 7 oxygen atoms | | | | | | | |
| Si | 1.738 | 1.909 | 1.991 | 1.755 | 2.235 | 1.879 | 1.942 |
| Ti | 0.001 | 0.000 | 0.001 | 0.002 | 0.003 | 0.003 | 0.001 |
| Al | 0.001 | 0.001 | 0.007 | 0.009 | 0.145 | 0.172 | 0.132 |
| Fe | 0.304 | 0.220 | 0.130 | 0.303 | 0.186 | 0.247 | 0.256 |
| Mn | 0.006 | 0.003 | 0.001 | 0.004 | 0.006 | 0.009 | 0.007 |
| Cr | 0.002 | 0.000 | 0.001 | 0.001 | 0.022 | 0.033 | 0.010 |
| Mg | 3.193 | 2.942 | 2.868 | 3.163 | 2.028 | 2.664 | 2.633 |
| Ca | 0.002 | 0.003 | 0.002 | 0.001 | 0.049 | 0.003 | 0.004 |
| Na | 0.001 | 0.002 | 0.001 | 0.001 | 0.001 | 0.000 | 0.000 |
| K | 0.000 | 0.000 | 0.002 | 0.000 | 0.000 | 0.000 | 0.000 |
| Ni | 0.012 | 0.010 | 0.002 | 0.000 | 0.004 | 0.004 | 0.001 |
| Fe+Mg | 3.50 | 3.16 | 3.00 | 3.47 | 2.21 | 2.91 | 2.89 |
| $X_{Fe}$ | 0.09 | 0.07 | 0.04 | 0.09 | 0.08 | 0.08 | 0.09 |
| Si+Al | 1.74 | 1.91 | 2.00 | 1.76 | 2.38 | 2.05 | 2.07 |

*Total Fe calculated as FeO.